The Raspberry Model for Hydrodynamic Interactions Revisited, Part I: Periodic Arrays of Spheres and Dumbbells

Lukas P. Fischer,[1] Toni Peter,[1] Christian Holm,[1] and Joost de Graaf[1,*]

[1] *Institute for Computational Physics (ICP), University of Stuttgart, Allmandring 3, 70569 Stuttgart, Germany*

(Dated: May 10, 2015)

The so-called 'raspberry' model refers to the hybrid lattice-Boltzmann and Langevin molecular dynamics scheme for simulating the dynamics of suspensions of colloidal particles, originally developed by [V. Lobaskin and B. Dünweg, New J. Phys. **6**, 54 (2004)], wherein discrete surface points are used to achieve fluid-particle coupling. This technique has been used in many simulation studies on the behavior of colloids. However, there are fundamental questions with regards to the use of this model. In this paper, we examine the accuracy with which the raspberry method is able to reproduce hydrodynamic interactions when compared to analytic expressions for a solid sphere in simple-cubic crystals. To this end, we consider the quality of numerical experiments that are traditionally used to establish these properties and we discuss their shortcomings. We show that there is a discrepancy between the translational and rotational mobility reproduced by the simple raspberry model and present a way to numerically remedy the problem by adding internal coupling points. Finally, we examine a non-convex shape, namely a colloidal dumbbell, and show that the filled raspberry model replicates the desired hydrodynamic behavior in bulk for this more complicated shape. Our investigation is continued in [J. de Graaf, *et al.*, XX **XX**, xx (2015)], wherein we consider the raspberry model in confining geometry of two parallel plates.

I. INTRODUCTION

The physical description of hydrodynamic interactions in fluids has been a field of intensive study for over three centuries. The first mathematical description of (rarified) flow dates back to Euler. [1] This description was subsequently refined by Navier and Stokes to be applicable to the flow of dense media. [2, 3] However, finding solutions to the Navier-Stokes equations, even under the simplifying assumption of the low Reynolds number regime, has proven to be a particularly challenging boundary-value problem. Only in a few simple geometries can the Navier-Stokes equations be analytically solved, often leading to truncated series expansions rather than a full solution.

Two geometries that can be handled semi-analytically are a simple-cubic array of spheres and a sphere between two parallel plates. The former is of particular interest as a toy model for fluid flow in a porous medium (at small sphere separations), [4] while the latter is relevant to, for example, the field of hydrodynamic chromatography. [5, 6] In this paper, we consider the crystalline arrangement and in Ref. [7] we study the confining geometry of two parallel plates.

There are a large number of (semi-)analytic investigations for the simple-cubic geometry, which makes this geometry perfectly suited for benchmarking the quality of hydrodynamic solvers. For the translational movement of a simple-cubic crystal through a fluid, the first results were obtained by Hasimoto, who derived a semi-numerical result for dilute systems. [8] A complete numerical study for a larger range of lattice spacings and various crystal structures was later presented by Zick and Homsy. [9] The hydrodynamic flow around an infinite (simple-cubic) array of rotating spheres was first described by Brenner *et al.* [10] These results were subsequently refined by Zuzovsky *et al.* [11] A complete numerical study of both translational and rotational friction over a large range of possible lattice spacings was provided by Hofman *et al.* [4] We utilize this large volume of data as a reference throught our manuscript.

A breakthrough in the numerical simulation of fluid dynamics resulted from the development of the lattice-Boltzmann (LB) algorithm. LB is based on the discretized version of the Boltzmann transport equation, see Ref. [12] for a brief background. This lattice-based algorithm allows for the efficient simulation of hydrodynamic interactions in arbitrary geometries using simple boundary conditions, such as the bounce-back rule to obtain no-slip surfaces. [12]

In the early days of LB, stationary bounce-back rules were introduced to describe boundaries. However, it proved difficult to extend the use of these grid-based boundaries to describe moving objects. One attempt to tackle the problem of moving particles was introduced by Ahlrichs and Dünweg, who simulated polymer chains by utilizing an interpolated point-coupling scheme. [13] These points couple to the fluid through a frictional force, acting both on the solvent and on the solute, which depends on the relative velocity. The effect of this coupling is the formation of a hydrodynamic hull around the points, which thus gain a finite hydrodynamic extent (effective hydrodynamic radius). [13] Even if individual friction coefficients and thus different effective radii are used for the points, this method is limited in the effective size ratios that it can handle, namely, by the particle-grid interpolation scheme and discretization used for the LB fluid. [13] Thus the method cannot be used to study systems spanning approximately one order of magnitude in

* jgraaf@icp.uni-stuttgart.de

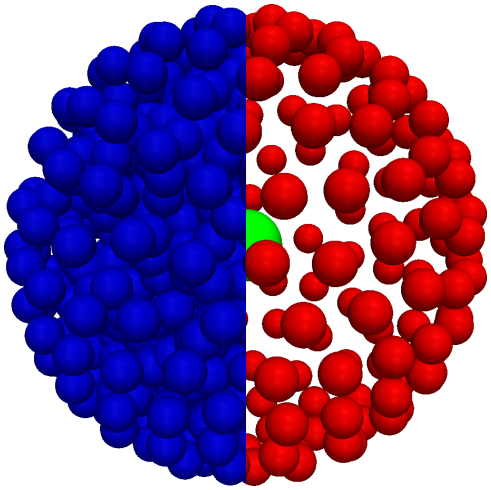

FIG. 1. (color online) Representation of the structure of the raspberry models used in our simulations, filled (left) and hollow (right), respectively. The central bead to which all other beads are connected *via* rigid bonds, is shown using a green sphere. The blue spheres represent the beads that form the filled raspberry and the red ones give the surface beads used for the hollow variant. The radius of the beads is chosen to be smaller than the typical effective hydrodynamic radius to help visualize the internal structure.

length, *e.g.*, the electrophoresis of colloids with explicit ions.

Lobaskin and Dünweg remedied this issue by introducing the so-called 'raspberry' model, in which a larger colloid is modeled using the aforementioned coupling by discretizing the surface of the colloid into points. [14] The method derives its name from this discretized nature of the surface, which resembles a raspberry, when represented by molecular-dynamics (MD) beads, see Fig. 1. A proper coverage of the surface by coupling points, such that the fluid inside of the shell is 'trapped' and thus translates and rotates in unison with the shell, was assumed to create an effective no-slip/co-moving boundary condition at the surface. [14, 15]

Moving bounce-back (as well as other varieties of) boundary conditions were subsequently developed to exploit the lattice structure of the LB in describing colloidal particles. [16, 17] However, the raspberry method has remained popular, because of its simplicity as a straightforward extension of point-particle coupling. It has been extended upon [15] and has been used in a wide variety of simulation settings. [18–20] Recently, this model was employed in the context of multi-particle collision dynamics (MPCD), [21, 22] stochastic rotation dynamics (SRD), [23] and dissipative particle dynamics (DPD) simulations. [24, 25]

Of singular interest are a set of recent publications from the Denniston group. [26–29] In these publications the quality of the (raspberry-type) point-coupling schemes are investigated and compared to theoretical expressions. Ollila *et al.* show in Ref. [26] that there is good correspondence between the LB simulations and analytic results [30, 31] for a hollow shell, an annulus, and a dense distribution of coupling points. They place these results in the context of the simulation of porous particles. In Ref. [27], Ollila *et al.* further analyzed the quality of the point-coupling method and showed that there are problems with this scheme when utilizing it to describe solid particles. In particular, Ollila *et al.* demonstrated that the hydrodynamic radius of these particles is ill-defined in an LB fluid. That is, the effective hydrodynamic radius that follows from the translational mobility (*via* the Stokes-Einstein relation) does not match that obtained using the rotational mobility. By careful calibration, [27] the use of a colloid radius that is 'incommensurate' with the lattice spacing, [26] and modification of the coupling of the points to the LB fluid, [28, 29] the rotational and translational effective radii can be well-matched and coincide with the radius given to the coupling points.

In this manuscript, we re-examine the raspberry model by Lobaskin and Dünweg [14] in the context of the work of Ollila *et al.* [26, 27] We show that there is a simple way to obtain an effectively consistent hydrodynamic description of a solid particle using the raspberry model, namely by introducing coupling points to the interior of the raspberry particle and fitting for the radius of a solid particle using suitable experiments, which we will describe. This 'filling + fitting' procedure does not necessitate a particle radius that is incommensurate with the lattice. Moreover, it yields an internally consistent formalism, which reproduces the hydrodynamic properties of a solid object to a high degree of accuracy.

We show how our fit parameter (the effective hydrodynamic radius) can be straightforwardly determined. To demonstrate that our method works for a range of reasonable LB parameters, we examine the quality of the raspberry model in the classic fluid-dynamics geometry of a simple-cubic arrangement. [4, 8, 10, 11] We show that the raspberry model reproduces the theoretical result surprisingly well for the complete range of applicable raspberry separations. In obtaining these results, we also analyze the quality of the standard hydrodynamics experiments performed in this geometry. [14, 15] We further demonstrate that the improved correspondence between the effective rotational and translational hydrodynamic radius is upheld over a large range in viscosity. Finally, we consider the effectiveness of the raspberry description for modeling a solid non-convex particles and show that the 'filled + fitted' model gives accurate results for the bulk mobility of a dumbbell-shaped colloid. Part II of our analysis, which extends these conclusions to raspberry particles under confinement, is presented in Ref. [7]. We thus demonstrate that for a wide range of suitably chosen parameters our 'filling + fitting' formalism leads to a substantially improved (and acceptable) numerical tolerance in simulating solid objects with respect to that of the traditional raspberry model of Refs. [14, 15].

The reason why adding internal coupling points is so

effective, is that the permeability (sometimes referred to as 'leakiness' in the context of the raspberry method) is substantially reduced, as was also observed in Ref. [26]. In other words, the Brinkman screening length that is only modulated by the coupling points at the surface of the traditional raspberry model, [14, 15, 27, 29] is now imposed throughout the volume. This sufficiently enhances the raspberry-fluid coupling to allow for these porous particles to be used to model solid objects. The 'filling + fitting' formalism has advantages over the method proposed by Refs. [27, 29] which achieves consistency by modifying the surface density only, as well as the method of Ref. [26] that requires incommensurability of the particle radius with the LB lattice. Moreover, we find that our procedure is effective for far lower coupling-point numbers than were utilized in Refs. [26, 27, 29], which is interesting from a computational efficiency perspective.

The remainder of this manuscript is structured as follows. In Section II we describe our simulation methods in detail. Section II A introduces our variant of the raspberry model for the spherical and dumbbell-shaped colloids of interest. Sections II B and II C detail the molecular dynamics and LB simulation parameters, respectively. Section II D describes the various hydrodynamic experiments that we performed to determine the properties of the raspberry model. We provide a summary of the notations used throughout the text in Section II E to aid the reader when going through the manuscript. In Section III we list our main results. We begin by examining the properties of the spherical raspberry in a simple-cubic lattice in Section III A. We continue with the properties of two dumbbell-shaped raspberries in Section III B. The results are discussed and related to previous studies in Section IV. Finally, we give a summary, conclusions, and an outlook in Section V.

II. METHODS

In this section, we outline the approach used to determine the hydrodynamic properties of a colloid. We have split this into subsections detailing the properties and construction of the raspberry model, the molecular dynamics and lattice-Boltzmann parameters used, the hydrodynamic experiments performed to extract the mobility of the raspberry, and a reference list of the input parameters and measured quantities.

A. The Raspberry Model

In this manuscript we study the so-called 'raspberry' model for particle-fluid interactions, [14] also see Fig. 1. This model relies on discretizing the surface of a larger colloid into coupling points, which experience a friction force related to the relative velocity of the fluid and the points. [13] In Ref. [14], 100 points were used to approximate a sphere. To ensure a reasonably homogeneous surface coverage these were connected to each other by finite extensible nonlinear elastic (FENE) potentials. The forces acting on the surface beads were forwarded to a central Lennard-Jones (LJ) MD bead, *via* the LJ interaction. A model similar in spirit to the one proposed by Lobaskin and Dünweg was developed by Chatterji and Horbach. [15] In their construction the surface beads were fixed with rigid bonds to the central bead and no FENE potential was employed for the surface-center coupling.

1. The Hollow Raspberry

For the construction of the raspberry model in this paper, we combined the approaches of Refs. [14, 15]. To arrange the MD beads in a spherical shell of radius R, we used a separate MD simulation. We placed $N \gtrsim \lceil 4\pi R^2/a^2 \rceil$ MD beads in a cubic simulation box with edge length L, LB lattice spacing a, and periodic boundary conditions. The number of MD beads was thus chosen such that on average there is at least one particle per lattice site for the LB simulation. To force the beads onto a spherical shell we employed a shifted harmonic bond potential around the center of the box (of the future particle) $\mathbf{r}_P$. This potential has the form

$$V_{\mathrm{harm}}(\mathbf{r}) = \frac{1}{2} K \left(|\mathbf{r} - \mathbf{r}_P| - R \right)^2 , \tag{1}$$

where $\mathbf{r}$ is a point in space and K is the spring constant. To ensure that the beads do not overlap and to homogenize the surface density, we endowed them with a repulsive Weeks-Chandler-Anderson (WCA) interaction potential

$$V_{\mathrm{WCA}} = \begin{cases} 4\epsilon \left(\left(\frac{\sigma}{r} \right)^{12} - \left(\frac{\sigma}{r} \right)^{6} + \frac{1}{4} \right) & r < 2^{1/6}\sigma \\ 0 & r \geq 2^{1/6}\sigma \end{cases} , \tag{2}$$

where σ is the MD base unit of length and is equal to the bead diameter.

The MD beads were thermalized using a Langevin thermostat with 'temperature' 1ϵ and friction coefficient $\Gamma = 1\tau^{-1}$. Here, ϵ is the MD base unit of energy and corresponds to $1k_{\mathrm{B}}T$, where k_{B} is the Boltzmann constant and T is the temperature, and τ is the MD base unit of time. The MD beads were given mass $1m_0$, with m_0 the MD base unit of mass ($m_0 = \tau^2\epsilon/\sigma^2$). By geometrically increasing the spring constant from $K = 1\epsilon$ to $K = 3{,}000\epsilon$ the MD beads are forced onto the spherical shell described by the potential in Eq. (1). We increased K by a factor of 1.1 to its final value of $K = 3{,}000\epsilon$ over 100,000 integration steps of length $\Delta t = 0.003\tau$. These simulations were performed using the MD software package *ESPResSo*. [32, 33] Finally, small deviations of the MD beads' radial position with respect to the desired distance R were removed by adjusting their radial position. The configuration was then 'frozen in' by connecting all beads to a central bead via rigid bonds (virtual sites). [33]

To test the quality of the result, the raspberry was checked for large holes in the surface coverage by applying a 'shotgun' algorithm. We randomly picked 50,000 points on the surface of the sphere and calculate the distances to the nearest surface bead. We arrived at the distribution of MD beads that we used throughout our simulations, by repeating this procedure with different initial configurations and particle numbers, until we found a system for which the maximum hole size was roughly 1σ (bead diameter). The outcome for a sphere of radius $R = 3\sigma$ is shown in the right-hand side of Fig. 1. Here, 202 surface beads were used to obtain a maximal hole diameter of 1.1σ. We refer to this model as a 'hollow raspberry' for the remainder of this manuscript.

2. *Filling the Raspberry*

We 'fill' the hollow-shell raspberry particle by adding coupling points in the interior, as outlined in detail below. We first formed a hollow raspberry according to the recipe in Section II A 1. Next, we added $N' \gtrsim \lceil 4\pi(R-\sigma/2)^3/3a^3 \rceil$ beads to the interior of the shell, which interact with each other and the shell MD beads via the WCA potential of Eq. (2). The force between the internal beads themselves was initially capped to $1\epsilon/\sigma$ to prevent numerical instabilities. The system was allowed to evolve by making use of a Langevin thermostat ($k_{\mathrm{B}}T = 1\epsilon$, $\Gamma = 1\tau^{-1}$). For the simulation, over 50,000 time steps of length $\Delta t = 0.005\tau$ were used during which the capping value was slowly raised to 100ϵ. This generally resulted in a random configuration with a homogeneous distribution of MD beads within the raspberry. These particles were subsequently frozen in place by adding rigid (virtual) bonds to the central MD bead.

We examined several values of N' and investigated the homogeneity of the distribution of MD beads. We settled upon a value of $N' = 722$, resulting in a total of $N_{\mathrm{tot}} = N + N' + 1 = 925$ MD beads for the so-called 'filled raspberry' of radius $R = 3\sigma$. This result is shown in the left-hand side of Fig. 1. Note that we used exactly the same hollow shell to construct our filled variant. Finally, it should be remarked that in the hydrodynamic simulations utilizing the raspberry model, all WCA interactions were switched off and only the rigid (virtual) bonds remained.

3. *Constructing a Dumbbell Raspberry*

A dumbbell-shaped raspberry model (filled or hollow) is constructed using a procedure that is analogous to the one given in Sections II A 1 and II A 2. Instead of a central harmonic potential, we used two harmonic potentials centered on $\mathbf{r}_P = (0, 0, -d/2)$ and $\mathbf{r}'_P = (0, 0, d/2)$, with d the distance between the sphere centers of the dumbbell (the length is $d+2R$). In addition, a WCA potential had to be added to prevent particles from accumulating in the neck of the dumbbell – the region where the two dumbbell spheres overlap, if $d < 2R$. To accomplish this, we used a WCA potential between the center of the dumbbell, located at $(0, 0, 0)$, and the surface MD beads. This potential had the following form

$$V_{\mathrm{neck}} = \begin{cases} 4\epsilon\left(\left(\frac{w}{r}\right)^{12} - \left(\frac{w}{r}\right)^{6} + \frac{1}{4}\right) & r < 2^{1/6}w \\ 0 & r \geq 2^{1/6}w \end{cases}, \quad (3)$$

where w is the width of the neck and is given by

$$w = \sqrt{R^2 - \frac{d^2}{4}}. \quad (4)$$

After letting the particles become trapped in the dumbbell shell, in the same manner as for the spherical shell, they are connected *via* rigid bonds to a particle at the geometric center of the dumbbell. The dumbbell may be filled with N' additional beads using the procedure outlined in Section II A 2. In this paper, we consider two dumbbell-shaped raspberry particles – one with $d = 5\sigma$ and one with $d = 7\sigma$ – corresponding to a partially overlapping configuration and one with the spheres just touching, respectively; see Fig. 2. We used ($N = 416$, $N' = 598$) for $d = 5\sigma$ and ($N = 502$, $N' = 404$) for $d = 7\sigma$, respectively, to ensure a homogeneous surface distribution and filling of the volume.

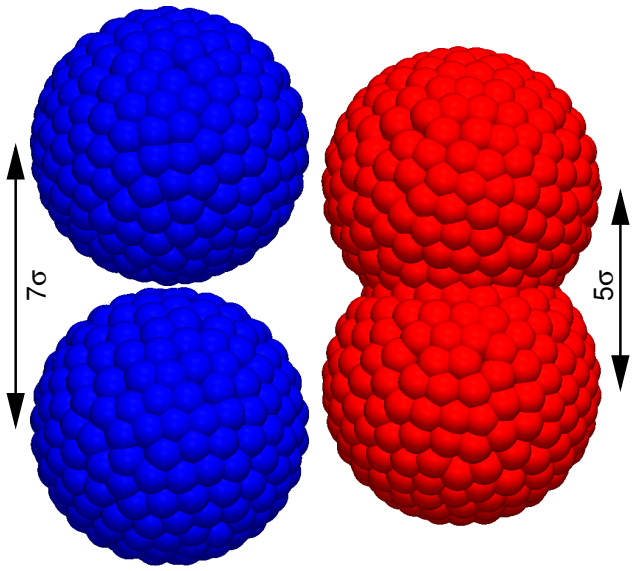

FIG. 2. (color online) Representation of the raspberry dumbbells used in our simulations, touching (left) and overlapping (right), respectively. The distance between the centers of the spheres (each $R = 3\sigma$ in size) is indicated using the arrows. Note that we used the effective MD bead diameter of approximately 1σ to visualize our result.

B. Molecular Dynamics Parameters

Once we had constructed the raspberries, we could use them in our LB simulations. The particles were allowed to freely move and rotate, unless otherwise specified. All the forces acting on the MD beads are transferred to the central bead *via* the virtual sites (rigid bonds). To stabilize the simulation for the bare friction coefficients used, we set the (bare) mass and rotational inertia of the raspberry; these quantities should not be confused with the virtual mass of the body in a fluid, see, *e.g.*, Ref. [34] for the definition. The mass and rotational inertia are based on the particle's dimensions and the fluid mass density, which we denote by ρ and set to $\rho = 1 m_0 \sigma^{-3}$. Here, we thus assume that the raspberry particle has the same density as the surrounding fluid.

For the sphere, the mass we used is $m = (4/3)\pi\rho R^3 \approx 113 m_0$ and the inertia tensor is a diagonal tensor with identical entries of $I = (8/15)\pi\rho R^5 \approx 407 m_0\sigma^2$. For the two dumbbell raspberries, we used

$$m = \begin{cases} \pi\rho\left(\frac{4}{3}R^3 + dR^2 - \frac{1}{12}d^3\right) & 0 \le d < 2R \\ \frac{8}{3}\pi\rho R^3 & d \ge 2R \end{cases} . \quad (5)$$

For the dumbbell, the rotational inertia tensor is diagonal, but the entries are not identical. Let $I_\parallel$ denote the moment for rotation about the main axis of the dumbbell and $I_\perp$ the moment for rotation about a central axis perpendicular to the main axis. We may then write

$$I_\perp = \begin{cases} \pi\rho\left(\frac{8}{15}R^5 + \frac{3}{4}dR^4 + \frac{1}{3}d^2R^3 + \frac{1}{24}d^3R^2 + \frac{1}{960}d^5\right) & 0 \le d < 2R \\ \pi\rho\left(\frac{8}{15}R^5 + \frac{2}{3}d^2R^3\right) & d \ge 2R \end{cases} ; \quad (6)$$

$$I_\parallel = \begin{cases} \pi\rho\left(\frac{16}{15}R^5 + \frac{1}{2}dR^4 - \frac{1}{12}d^3R^2 + \frac{1}{160}d^5\right) & 0 \le d < 2R \\ \frac{16}{15}\pi\rho R^5 & d \ge 2R \end{cases} ; \quad (7)$$

$$\underline{\underline{I}} = \begin{pmatrix} I_\perp & 0 & 0 \\ 0 & I_\perp & 0 \\ 0 & 0 & I_\parallel \end{pmatrix} , \quad (8)$$

where the long axis of the dumbbell is assumed to be aligned with the z-axis. This gives us the following for the $d = 5\sigma$ dumbbell: $m \approx 221 m_0$, $I_\perp \approx 2226 m_0\sigma^2$, and $I_\parallel \approx 810 m_0\sigma^2$. Whereas for the $d = 7\sigma$ dumbbell we obtain: $m \approx 226 m_0$, $I_\perp \approx 3585 m_0\sigma^2$, and $I_\parallel \approx 814 m_0\sigma^2$.

C. Lattice-Boltzmann Parameters

The raspberry particles were coupled to a LB fluid. We used a graphics processing unit (GPU) based LB solver, [35] which is attached to the MD software *ESPResSo*. [32, 33] The GPU variant of LB implemented in *ESPResSo* utilizes a D3Q19 lattice and a fluctuating multi-relaxation time (MRT) collision operator. [36] This fluctuating LB model was introduced first by Adhikari *et al.* [37] and later validated by Dünweg *et al.* [38, 39] The particle-fluid interaction proposed by Ahlrichs and Dünweg [13] was used to couple the fluid to embedded MD beads. We did not employ the coupling scheme of Refs. [28, 29], since our method turned out to work sufficient well for the long-time properties without modifications to the Ahlrichs and Dünweg LB coupling. The particle coordinates were interpolated onto the lattice using a tri-linear scheme. [12]

To keep our result as general as possible, we set the density of the fluid to $\rho = 1 m_0\sigma^{-3}$, the lattice spacing to 1σ, the time step to $\Delta t = 0.005\tau$, the (kinematic) viscosity to $\nu = 1\sigma^2\tau^{-1}$, the bare particle-fluid friction to $\zeta_0 = 25\tau^{-1}$, and the strength of the fluctuations to $k_\mathrm{B}T = 0.01\epsilon$, unless otherwise specified. Here, we chose neither to optimize our parameters for the most accurate reproduction of hydrodynamic interactions, nor to match a specific experimental system of interest *via* telescoping. [40, 41] The reason behind our choice is to use parameters that are in the regime, where LB reproduces hydrodynamic effects reasonably well and is sufficiently stable to use the (float-precision) GPU algorithm; thus making our results 'generic' rather than tailored to a specific system. The low amplitude of the fluctuations in the thermalized LB is to allow averaging over long times without noise dominating our results, as will become more clear when we discuss these and prove important for the thermal averaging performed in Ref. [7] as well.

D. Hydrodynamic Experiments

To assess the quality of the raspberry approximation in modeling the hydrodynamic properties of a colloid we performed several experiments. We use the term 'quiescent' to describe an un-thermalized (non-fluctuating) LB fluid. Below we specify the experiments performed for particles in a simple cubic lattice, *i.e.*, a cubic simulation box of length L with periodic boundary conditions. In all experiments the particle was initialized in the center of the box.

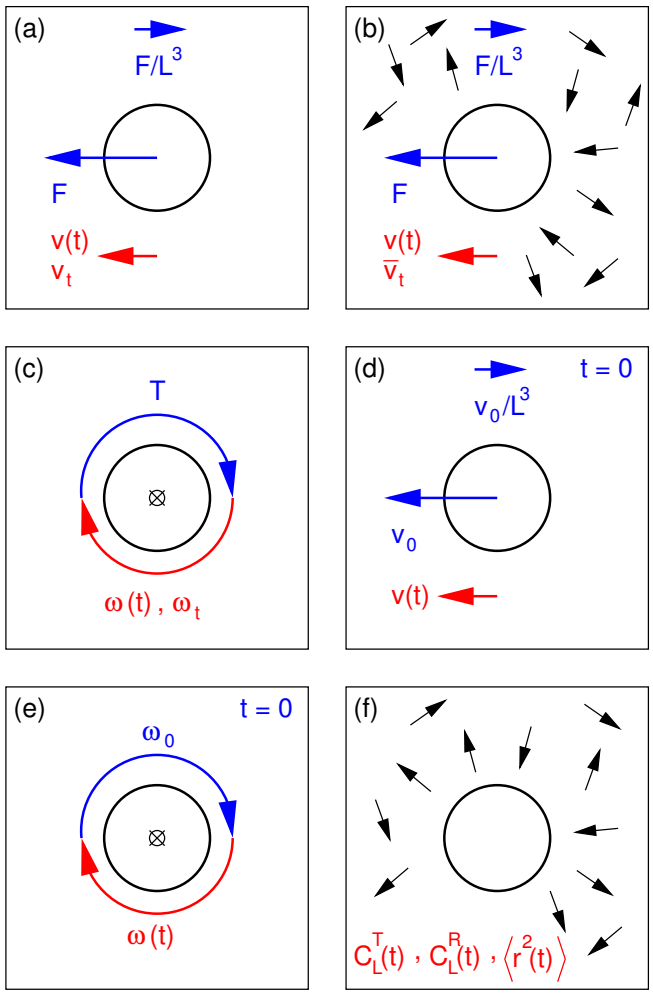

FIG. 3. (color online) Visualization of the various hydrodynamic experiments carried out in a cubic box of length L with periodic boundary conditions. A two-dimensional (2D) representation is given here. The blue arrows and symbols denote quantities applied to the fluid and raspberry, the red arrows and symbols indicate measured quantities. The black arrows indicate a thermalized fluid. We refer to the text for a description of the experiments, as well as the applied and measured quantities.

- A *force* experiment in a quiescent fluid, see Fig. 3(a). A constant force $\mathbf{F}$ was applied to the particle (typically along one of the box axes) and a counter force density of $-\mathbf{F}/L^3$ was applied homogeneously to the fluid to ensure that there is no motion of the center of mass, *i.e*, no net transfer of momentum to the system. Not applying this counter force density would result in an acceleration of the colloid *via* the fluid flow that builds up, as momentum is continuously pumped into the system. The resulting time-dependent velocity $\mathbf{v}(t)$ and steady-state (terminal) velocity $\mathbf{v}_t$ were measured and used to determine the translational mobility

$$\mu_L^T = \frac{|\mathbf{v}_t|}{|\mathbf{F}|}. \tag{9}$$

- A *force* experiment in a thermalized fluid, see Fig. 3(b). The set-up is the same as for the first experiment. However, the system was first equilibrated until a steady-state emerged and the particle fluctuated with the proper thermal distribution. During the production run, $\mathbf{v}(t)$ was averaged to determine the average steady-state velocity $\bar{\mathbf{v}}_t = \langle \mathbf{v}(t) \rangle$, where $\langle \cdot \rangle$ denotes the time average. This allowed us to determine the time-averaged translational mobility

$$\bar{\mu}_L^T = \frac{|\bar{\mathbf{v}}_t|}{|\mathbf{F}|}. \tag{10}$$

- A *torque* experiment in a quiescent fluid, see Fig. 3(c). A constant torque $\mathbf{T}$ was applied to the particle (typically along one of the box axes). The resulting time-dependent angular velocity $\boldsymbol{\omega}(t)$ and steady-state angular velocity $\boldsymbol{\omega}_t$ were measured and used to determine the rotational mobility

$$\mu_L^R = \frac{|\boldsymbol{\omega}_t|}{|\mathbf{T}|}. \tag{11}$$

  There is no need to apply a 'back torque density' to the fluid in this experiment, as the periodic boundary conditions do not allow the fluid to develop a net rotation.

- A *velocity* experiment in a quiescent fluid, see Fig. 3(d). An instantaneous velocity $\mathbf{v}_0$ was imparted onto the particle at $t = 0$ and an instantaneous counter velocity of $-\mathbf{v}_0/L^3$ was applied homogeneously (at the same time) to the fluid to ensure zero net motion of the system. The resulting time-dependent velocity $\mathbf{v}(t)$ was measured. This quantity can be related to a de-dimensionalized velocity auto-correlation function (VACF) $C^T(t)$ *via* the relation

$$C_L^T(t) = \frac{\mathbf{v}_0 \cdot \mathbf{v}(t)}{|\mathbf{v}_0|^2}, \tag{12}$$

  where $\cdot$ denotes the dot product.

- An *angular velocity* experiment in a quiescent fluid, see Fig. 3(e). An instantaneous angular velocity $\boldsymbol{\omega}_0$ was imparted onto the particle at $t = 0$. The resulting time-dependent angular velocity $\boldsymbol{\omega}(t)$ was measured. This quantity can be related to a dedimensionalized angular velocity auto-correlation function (AVACF) $C^R(t)$ *via*

$$C_L^R(t) = \frac{\boldsymbol{\omega}_0 \cdot \boldsymbol{\omega}(t)}{|\boldsymbol{\omega}_0|^2}. \tag{13}$$

- An *auto-correlation* experiment in a thermalized fluid, see Fig. 3(f). The system was equilibrated until the particle fluctuated with the proper thermal distribution. The (A)VACF and the mean square displacement (MSD) were measured using the multiple-tau correlator in *ESPResSo*. [42] For the (A)VACF the (angular) velocity in the co-rotating frame was averaged. The $C^T(t) \equiv \langle \mathbf{v}(t) \cdot \mathbf{v}(t+\tau) \rangle$ and $C^R(t) \equiv \langle \boldsymbol{\omega}(t) \cdot \boldsymbol{\omega}(t+\tau) \rangle$ that follow from the thermal experiments differ slightly from those in Eqs. (12) and (13), since $C^T(0) = 3k_\mathrm{B}T/m$ and $C^R(0) = 3k_\mathrm{B}T/I$, as a consequence of the equipartition theorem. This allows us to compute the translational and rotational mobility, respectively, *via* the Green-Kubo relation

$$\mu_L^X = \frac{1}{3k_\mathrm{B}T} \int_0^\infty C^X(t)\mathrm{d}t, \tag{14}$$

where the factor 1/3 is used for spherical particles only and X can be either T or R. [43] The relations for anisotropic particles are similar, but slightly more involved, since the dot product for the (A)VACF is replaced by the dyadic product.

In the above experiments, care was taken to ensure that the particle remained in the low translational Reynolds number regime

$$Re^T = \frac{vR}{\nu} \ll 1, \tag{15}$$

with v the maximum/typical velocity. This implies that we can compare it to analytic and numerical results obtained by solving the Stokes equations, as will be discussed further in Section III. For the radius $R = 3\sigma$ colloid and our value of the kinematic viscosity, we ensured that the maximum particle velocity remained under $0.15\sigma\tau^{-1}$, for which $Re^T < 0.5$. However, this value was only attained in the *velocity* and *auto-correlation* experiments in the cubic geometry for the first time step. For $t \gg 1\tau$ and in the other experiments, the Reynolds number remained smaller than 0.1. Similarly the rotational Reynolds number

$$Re^R = \frac{\omega R^2}{\nu}, \tag{16}$$

with ω the maximum angular velocity, remained small: $Re^R < 0.7$, but typically smaller than 0.1.

E. Notations Used throughout this Manuscript

In this section, we summarize the notations used in this manuscript. This will aid the reader in going through the text, as many of the notations are necessarily similar.

- L, the box length of a cubic box with periodic boundary conditions.
- R_h^T, the effective hydrodynamic radius obtained by extrapolating translational mobility measurements, see Figs. 3(a,b,d,f), for the limit of box length $L \uparrow \infty$. The subscript h is used to differentiate R_h from the bead-to-center distance of the raspberry's coupling points R.
- R_h^R, the effective hydrodynamic radius obtained by extrapolating rotational mobility measurements, see Figs. 3(c,e,f), for the limit of box length $L \uparrow \infty$.
- $C_L^T(t)$, the velocity auto-correlation function (VACF) for translational movement in a cubic box of length L with periodic boundary conditions, also see Figs. 3(d,f) and Eq. (12).
- $C_L^R(t)$, the angular velocity auto-correlation function (AVACF) for rotation in a cubic box of length L with periodic boundary conditions, also see Figs. 3(e,f) and Eq. (13).
- $\mu_L^T(t)$, the time-dependent translational mobility in a cubic box of length L with periodic boundary conditions, also see Fig. 3(a). When the time dependence is dropped the limit $t \uparrow \infty$ has been taken.
- $\mu_L^R(t)$, the time-dependent rotational mobility in a cubic box of length L with periodic boundary conditions, also see Fig. 3(c). When the time dependence is dropped the limit $t \uparrow \infty$ has been taken.
- $\bar{\mu}_L^T$, the time-averaged translational mobility resulting from the thermal force experiment, also see Fig. 3(b).
- μ_0^T, the bulk translational mobility, which follows from the limit $L \uparrow \infty$ of μ_L^T.
- μ_0^R, the bulk rotational mobility, which follows from the limit $L \uparrow \infty$ of μ_L^R.
- f, the fractional deviation between two results.

III. RESULTS

In this section, we discuss the results that we obtained by performing the simulations and numerical calculations outlined in Section II. We have split these into two parts: one for the sphere and one for the dumbbell. These parts are further subdivided according to the nature of the experiments.

A. Sphere in a Simple Cubic Crystal

1. The (Angular) Velocity Auto-Correlation Function

Using the (quiescent) *velocity* and (thermalized) *auto-correlation* experiments discussed in Section II D, see Figs. 3(d,f), we established the VACF for a filled raspberry sphere in a cubic box of length $L = 100\sigma$. The results are shown in Fig. 4. From Figs. 4(a,b,c) we observe the three (possibly four) decay regimes that are typical for the LB simulations of the raspberry particle. In the following they will be described in more detail.

(I) At short times there is an unphysical-coupling regime, see Fig. 4(a), in which the VACF decays exponentially according to

$$\frac{C_L^T(t)}{C_L^T(0)} = \exp\left(-\frac{N_{\text{tot}}\zeta_0}{m}t\right), \tag{17}$$

with N_{tot} the total number of beads, ζ_0 the bare friction coefficient, and m the particle's (bare) mass. [14] The existence of this regime can be attributed to the fluid not co-moving with the velocity of the particles. That is, the MD beads interact with the stationary fluid only through a regular Langevin-type friction – the velocity of the fluid is essentially zero in these time steps.

The expected (unphysical) decay of Eq. (17) is indicated in Fig. 4(a) and matches reasonably well with the observed initial decay. However, the result deviates even in the first and second time step, signifying the onset of proper coupling. This is in agreement with the recent observations in the MPCD simulations of Ref. [22], where this deviation from the expected unphysical decay was also attributed to the onset of hydrodynamic correlations. Finally, note that there is a small deviation between the thermalized LB result and the quiescent VACF when $t > 0.03\tau$, to which we will come back later.

From the above it is thus clear that the no-slip boundary condition at the surface of the raspberry is violated at short times, even taking the finite compressibility of the LB fluid into account. Moreover, the expected decay for a porous colloid [44] is not captured by the raspberry with the Ahlrichs and Dünweg coupling [13] This is a problem inherent to the LB method. [14, 15] The modified coupling scheme by Mackay *et al.* [28] purportedly can be used to remedy this problem, we will come back to this in Section IV.

(II) At intermediate times there is a regime, in which the VACF decays exponentially according to Stokes' prediction

$$\frac{C_L^T(t)}{C_L^T(0)} \propto \exp\left(-\frac{6\pi\eta R}{m}t\right). \tag{18}$$

Here, we used the proportionality symbol, since the unphysical initial decay makes it impossible to establish an analytic prefactor for the onset of this regime in fluid-particle coupling. The regime appears because the hydrodynamic coupling between the particles and the surrounding fluid is now fully established. [14]

The match between Stokes' prediction and our numerical results can be appreciated in Fig. 4(b), where a Stokes-type decay has been fitted to our data. The agreement is not very convincing. However, the agreement between the bare-mass prediction of Eq. (18) is superior to the one in which the virtual mass is used [34] (not shown here); the latter type of decay was originally suggested by Lobaskin and Dünweg. [14] The superiority of the bare-mass result is reasonable, since Felderhof [44] has shown that for a porous sphere the virtual-mass decay regime is absent. Unfortunately, the porous sphere solution of Felderhof [44] does not match better in the Stokes-type regime, as the regime sets in after sound-waves have had sufficient time to propagate the size of the colloid (also see the next paragraph) due to the presence of the unphysical decay.

We have indicated three characteristic times related to sound propagation in the LB in Fig. 4(b). The speed of sound in LB is given by

$$v_s = \sqrt{\frac{1}{3}}\left(\frac{\sigma}{\Delta t}\right), \tag{19}$$

where σ is the lattice spacing, Δt is the time step, and the prefactor stems from the dimensionality of the grid. The three times are $t_\sigma = \sigma/v_s$, $t_{2R} = 2R/v_s$, and $t_L = L/v_s$, *i.e.*, the time required for sound waves to propagate one lattice spacing, the diameter of the raspberry, and the length of the box, respectively. We will now discuss the relevance of these times.

For the filled sphere, in which the MD beads are roughly 1σ apart, we find possible signatures of the propagation of sound between the MD beads, as can be inferred from the short-time oscillations. The first dip in the VACF roughly coincides with t_σ, as indicated by the black dashed line in Fig. 4(b). These oscillations may also be related to the magnitude of the effective friction that the added coupling points in the interior bring about. At the time it takes sound to propagate the diameter of the sphere (t_{2R}), we find a small dip in the VACF, see the dashed gray line in Fig. 4(b). This dip is similar to the one observed in Ref. [22] and is caused by the compressibility of the LB fluid. [34]

Note that the Stokesian regime of decay appears to be delimited by the time it takes sound to travel the distance of the box (t_L, dotted gray line in Fig. 4(b)). However, for our specific choice of parameters, this time is close to the viscous time it takes momentum to diffuse by one colloidal radius $t_\eta = \rho R^2/\eta = 9\tau$. This viscous time is the relevant time scale for the development of hydrodynamic memory effects. [34, 43] We have a stricter separation of sonic and viscous time scales than in Refs. [21, 22], *i.e.*, $t_\eta/t_{2R} \gg 1$. Therefore, our results do not display sound undulations (back tracking) in the long-time power-law regime.

(III) After a sufficiently long time, the hydrodynamic interactions with the surrounding fluid result in a persistence of the velocity (non-exponential decay) as the vorticity diffuses away from the particle. These hydro-

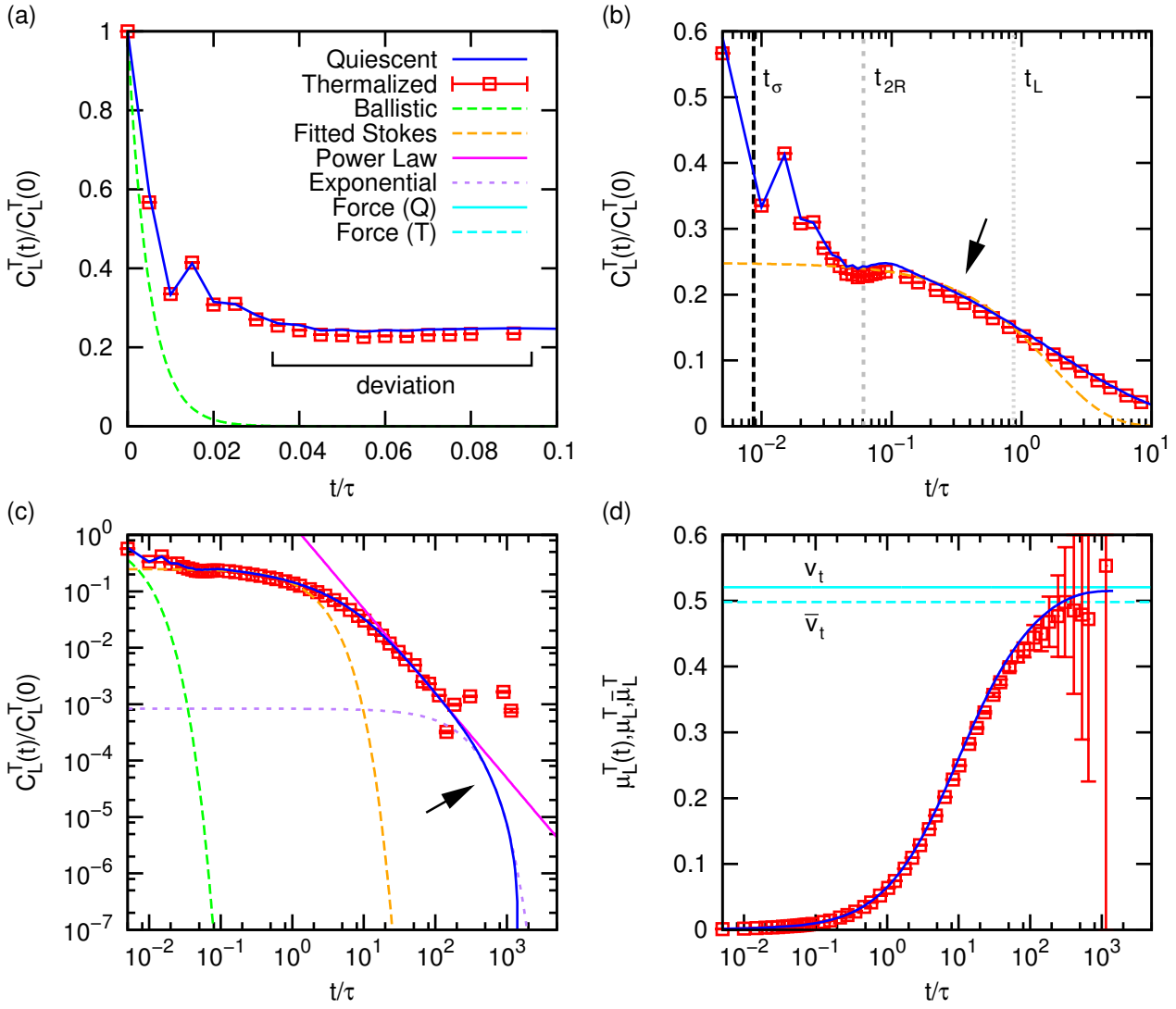

FIG. 4. (color online) The velocity auto-correlation function (VACF) $C_L^T(t)$ as a function of time t expressed in the MD time unit τ. The graphs show results for a filled raspberry of radius $R = 3\sigma$ in a box of length $L = 100\sigma$, with LB parameters as given in the text. (a) The initial decay of the VACF. The red squares with error bars show the result for a thermalized LB, the blue solid curve gives the result of a quiescent experiment, and the green dashed line shows the predicted unphysical-coupling decay inherent to LB. (b) Log-linear plot of the initial and intermediate decay of the VACF. The dashed orange curve gives the expected Stokes' decay. An arrow indicates the position where the correspondence is reasonable. The vertical lines indicate the time for sound waves to propagate through the system over certain lengths: one lattice spacing (t_σ, dashed black), roughly the inter-bead separation; the raspberry's hydrodynamic diameter (t_{2R}, dashed gray); and the box length (t_L, dotted gray). (c) Log-log plot of the long-time decay. The magenta line shows the power-law decay. The unphysical-coupling, fitted Stokes', and final exponential-decay (purple dashed, indicated by an arrow) curves are shown for completeness. (d) The time-dependent Green-Kubo value of the translational mobility $\mu_L^T(t)$ obtained from the quiescent (blue solid curve) and thermalized (red squares with error bars) LB result. The solid cyan line shows the result of a quiescent force experiment (μ_L^T, derived from the terminal velocity v_t), while the dashed cyan line shows the result of a thermal-averaged force experiment ($\bar{\mu}_L^T$, from the time-averaged terminal velocity $\bar{v}_t$).

dynamic memory effects lead to an algebraic decay of the (A)VACF; the so-called 'long-time tail'. [45] This decay has the following form

$$C_L^T(t) = \frac{1}{12} m\sqrt{\rho}(\pi\eta t)^{-3/2}; \tag{20}$$

$$C_L^R(t) = \pi I\sqrt{\rho}(4\pi\eta t)^{-5/2}, \tag{21}$$

for the translational and rotational motion, respec-

tively. [34, 43, 46, 47] Figure 4(c) shows this power-law decay for the translational motion more clearly. The correspondence with the quiescent data is excellent. Here, we additionally incorporated a prefactor that accounts for the finite size of the simulation box, using the Hasimoto scaling expression [8] to obtain a match for both the prefactor and exponent via a fitting procedure that is within 1% of the theoretical prediction. Note that within the error bar, which gives the standard error, the decay is captured by the thermalized result. The thermal data is not very convincing, but it was the best that could be achieved within a reasonable time frame for our choice of parameters. Only for $L \gg 30R$ is the regime, over which there is power-law decay, more pronounced, however, larger box sizes require even longer sampling. Our result is similar to the observations of Refs. [14, 15].

(IV) For the quiescent data, there is a third exponential decay in the data when $t \gg \tau$, see the purple dashed line in Fig. 4(c). Analysis shows that this decay has a small exponent that depends on the size of the simulation box. The exponential decay for $t \gg \tau$ is most likely (A) a numerical or (B) a method artifact. For the former (A), the decay could be due to the low velocity of both the particle and the fluid. It is conceivable that the velocity of the fluid decays faster than that of the particle, therefore causing another unphysical-coupling regime to set in. For the latter possibility (B), it could be that the back-velocity that is applied to the fluid in the quiescent experiment unfavorably affects the long-time tail. Indeed, this could explain why the exponent has box-size dependence. For the thermal data it is not possible to judge whether a third exponential regime sets in, since the error bar is too large. However, since the thermalized LB fluid has a far greater local flow profile than the quiescent result (for long times), it is likely that such a regime is absent in case (A). Since no back-velocity is applied to the fluid the regime would be absent if it is a method artifact (B).

Finally, we considered the Green-Kubo relation for the VACF by taking the anti-derivative

$$\mu_L^T(t) = \frac{1}{3k_\mathrm{B}T}\int_0^t C_L^T(t')\mathrm{d}t', \tag{22}$$

for the thermalized data. The expression for the quiescent data is similar. Figure 4(d) shows the resulting time-dependent translational mobility $\mu_L^T(t)$. We obtained the value of $\mu_L^T \equiv \mu_L^T(t \uparrow \infty) = 1.37 \cdot 10^{-2}\sigma^2\epsilon^{-1}\tau^{-1}$ from the quiescent data for the box of length $L = 100\sigma$. The data for the thermalized LB has a slightly lower value than the quiescent result, which can in part be attributed to the deviation that was already present at short times. In addition to determining μ_L^T from the VACFs we performed a quiescent and thermalized force experiment. The result is shown using the solid and dashed cyan lines in Fig. 4(d), respectively. We arrived at $\mu_L^T = 1.38 \cdot 10^{-2}\sigma^2\epsilon^{-1}\tau^{-1}$ for the quiescent data and $\bar{\mu}_L^T = 1.32 \cdot 10^{-2}\sigma^2\epsilon^{-1}\tau^{-1}$ for the thermalized data. The results from the VACF and the force experiments correspond within the error, but there is a discrepancy between the thermal and quiescent data. This deviation can be explained by the way these experiments are carried out and indicate a fundamental shortcoming of the quiescent experiments, as alluded to above and as will become more clear when we discuss the effect of box size in Section III A 2.

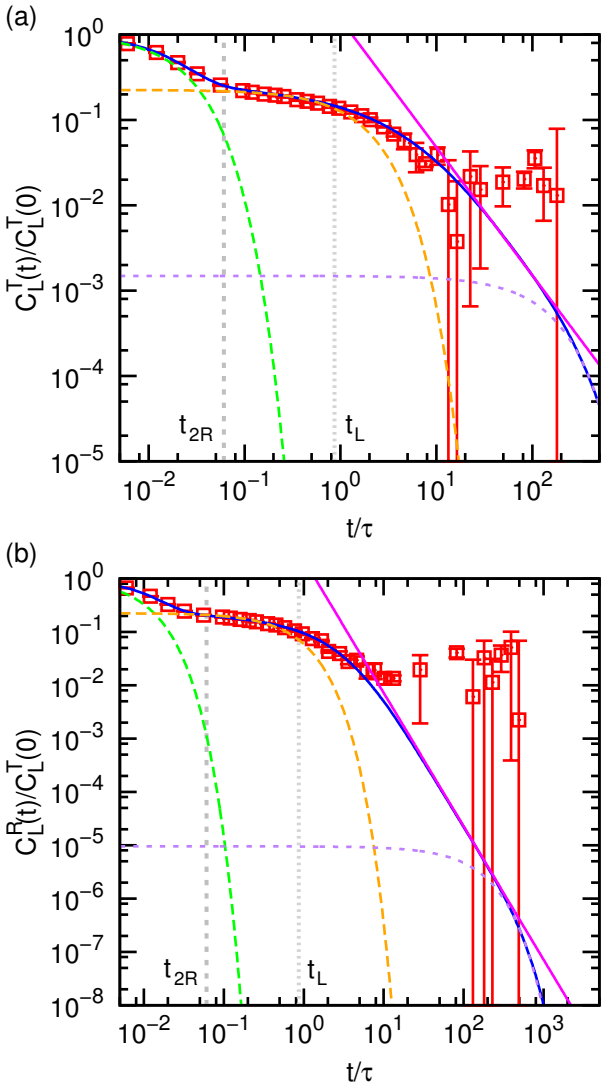

FIG. 5. (color online) Auto-correlation functions for a hollow raspberry of radius $R = 3\sigma$ in a box of length $L = 80\sigma$ as a function of time t expressed in the MD time unit τ. The LB parameters are as given in the text. The use of symbols is the same as in Fig. 4. (a) Velocity auto-correlation function (VACF) $C_L^T(t)$ for the thermal (red squares with error bars) and quiescent (blue curve) calculations. The unphysical-coupling (dashed green), the fitted Stokes decay (orange dashed), fitted final exponential-decay (purple dashed) curves, and power-law decay (magenta) are also shown. The two dashed vertical lines show the time it takes for sound to travel the particle's hydrodynamic diameter (t_{2R}, dashed) and the box length (t_L, dotted), respectively. (b) The angular-velocity auto-correlation function (AVACF) $C_L^R(t)$ for the same parameters.

In order to examine the difference between the hollow and filled raspberry model, we carried out similar experiments for a hollow-raspberry sphere in a box of length $L = 80\sigma$. We find similar regimes as in Fig. 4. For the hollow raspberry there is weaker coupling with fluid. This is caused by the spatial distribution of coupling points, not the amount of points, [26] as we will see in Section III A 2. This results in weaker decay of the unphysical-coupling regime, which therefore matches the exponential form of Eq. (17) more closely. Note that the existence of the power-law behavior is more convincingly shown by our AVACF data, see Fig. 5(b), as the fitted function and measured decay correspond well over a decade in time. The presence of the long-time exponential decay in the AVACF indicates that this third exponential decay is more likely an artifact of type (A) than of type (B), since no back torque is applied in this experiment. It is unclear whether the modified coupling scheme by Mackay *et al.* [28] shows a similar decay. Finally, it should be noted that for the hollow raspberry VACF there is the same deviation between the quiescent and thermalized LB results as shown in Fig. 4(a). However, the thermal and quiescent data for the AVACF match well throughout.

2. *The Influence of Lattice Spacing*

Thus far, we have examined only the results of the (angular) velocity experiments, and shown that these correspond – at least amongst themselves – to the results of force experiments for the same system. Let us now consider the effect of the lattice spacing of the simple cubic crystal on the hydrodynamic coupling between the spheres. This simple cubic geometry is unlike a physical crystal, in the sense that all particles translate and rotate in unison; an effect of there being only a single particle in a box with periodic boundary conditions. There is experimental evidence that such systems may be realized. [48–50] The uniformity of the periodic structure makes the solutions to Stokes' equations for this geometry analytically tractable. Such calculations were performed, for example, in the work of Hasimoto [8] and of Hofman *et al.* [4]

Figure 6(a) shows the change in velocity $v(t)$ during a force experiment, see Fig. 3(a), for a number of box sizes L using the filled raspberry model. Note that for larger L the friction experienced by the particle is smaller, as the hydrodynamic-interaction contribution of periodic images is reduced. However, the time it takes for the stationary state to set in is increased, as it takes longer to transfer momentum between the particle and its images. From the terminal velocities in the stationary state we determined the mobility.

In order to establish the mobility at infinite dilution (one particle in bulk), we fitted our data using a polynomial of the Hasimoto form $a + b/L + c/L^3$ [8] in the range where this form is expected to be valid and extrapolated to $L \uparrow \infty$. The resulting value for a is the bulk translational mobility

$$\mu_0^T \equiv \frac{1}{6\pi\eta R_h^T}, \tag{23}$$

with R_h^T the translational hydrodynamic radius. We were thus able to determine the extrapolated value μ_0^T and simultaneously the effective hydrodynamic radius of our raspberry colloid, using Eq. (23). This extrapolation refers to the 'fitting' part of our 'filling + fitting' formalism. These two parameters μ_0^T and R_h^T allowed us to de-dimensionalize the box length and the measured translational mobility, as shown in Fig. 6b.

In Figs. 6(b,c) we compare the quality of our result for the box-size dependence with the analytic result by Hasimoto [8] (dashed red curve) and the numerical calculations by Hofman *et al.* [4] (dashed green curve). Figure 6(c) shows the fractional deviation f between our data and the two literature results, as well as the difference between the Hasimoto (Ha) and Hofman *et al.* (Ho) data. For the data points provided by Hofman *et al.* [4] we used a polynomial fit of the form $1 + a/L + b/L^3$ to represent these as a curve. Note that the analytic and numerical expressions of Refs. [4, 8] correspond well for box sizes greater than $L \approx 5.0R_h^T$. That is, within the error that can be expected for the fitting procedure that we applied to the data by Hofman *et al.*, there is good agreement between their and Hasimoto's data over this range. The discrepancy for smaller box sizes can be explained by the truncation of the series expansion that was used in Hasimoto's work.

Our raspberry results (Ra) agree reasonably well with the data of Hofman *et al.* over the range $L \gtrsim 5.0R_h^T$, but there is also a clear signature of systematic deviation present in f. This implies that our data differs substantially from the values of Ref. [4] in the $1/L^3$ term. A similar range of agreement and small-box-size deviation can be observed between our data and that of Hasimoto. However, in spite of this, our data is much closer to the results of Hofman *et al.* than those of Hasimoto; by almost an order of magnitude in f for $L \downarrow 2R_h^T$. We will discuss the origin of the systematic deviation between our data and that of Ref. [4] next.

The discrepancy between our data and the result by Hofman *et al.* brings us back to the difference that we observed between the VACFs obtained from the velocity and temperature experiments carried out in Section III A 1, see Fig. 4(a). Remember that in the quiescent experiments a homogeneous and instantaneous velocity has to be applied to the fluid in order to ensure zero net movement of the system, see Fig. 3(d). Similarly, for the quiescent force experiment, a constant homogeneous force density is applied to the fluid, see Fig. 3(a). Consequently, this velocity and force are also applied directly to fluid nodes that are coupled to raspberry MD beads. The effective force applied to the colloid can therefore be calculated by subtracting the integrated fluid force-field

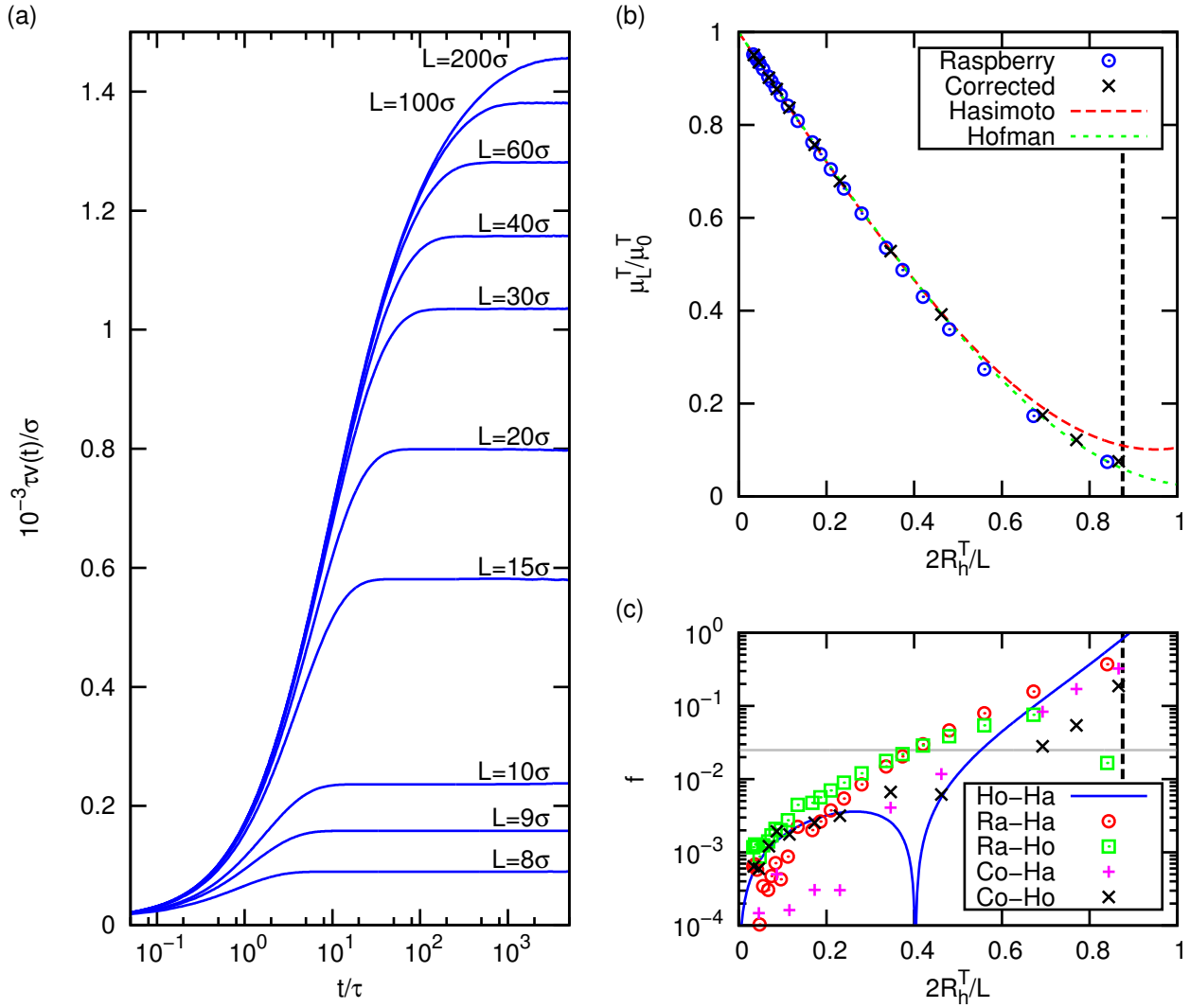

FIG. 6. (color online) (a) The velocity $v(t)$ as a function of time t expressed in the MD time unit τ obtained from force experiments for a selection of box sizes L. (b) The dependence of the particle's translational mobility μ_L^T (expressed in terms of the bulk translational mobility μ_0^T) on the inverse box length $1/L$ times the hydrodynamic diameter (twice the hydrodynamic radius R_h^T). The blue circles show results obtained from the velocity experiment. The black crosses give the results of the force experiment, corrected for the counter force applied inside of the raspberry, as explained in detail in the main text. The red dashed curve shows the analytic expression by Hasimoto [8] and the green dashed curve shows a polynomial fit to the numerical data of Hofman *et al.* [4] The vertical dashed black line indicates the value of L for which the spheres are separated by one lattice spacing ($L = 2R_h^T + \sigma$). (c) Fractional deviation f as a function of $2R_h^T/L$. The solid blue curve shows the difference between the theoretical expressions of Hasimoto and Hofman. The red circles and green squares indicate the difference between our raspberry experiment and the Hasimoto and Hofman expressions, respectively. The magenta pluses and black crosses give the difference between the force-corrected data and the Hasimoto and Hofman expressions, respectively. The gray horizontal line indicates a fractional deviation of 2.5%.

over the volume of the raspberry. This calculation yields

$$\mathbf{f}_{\text{eff}} = \mathbf{f}\left(1 - \frac{4\pi R^3}{3L^3}\right), \tag{24}$$

where $\mathbf{f}$ is the force directly applied to the central bead of our raspberry construct. Analogously, the counter velocity affects time evolution of the VACF. For the thermalized experiments this was not an issue, since counter velocities and forces do not need to be applied. These counter velocities and forces are therefore a likely candidate for the observed discrepancies. This implies that the force/velocity experiments are unsuited to analyze the hydrodynamic properties of finite systems in their present form. The fact that there is a mismatch between the thermal and quiescent results in Fig. 4(a) is thus not an expression of a violation of the equipartition theorem

or fluctuation dissipation. Nor is it correct to argue that this is a consequence of the porosity of the particle. The counter-force is only used to counter momentum transfer to the periodic system by the force applied to the particle. The behavior in the limit of the infinite system is, however, accurately captured, as the back velocity and force vanish.

We took the effective force of Eq. (24) to determine the 'corrected' value of μ_L^T (Co) using Eq. (9) as a function of the box size, see Fig. 6(b). Note that the correspondence between the result by Hofman *et al.* and our data is thus greatly improved and that the systematic deviation is removed for large box sizes. Moreover, for small box sizes the deviation between our corrected result and the literature values is substantially reduced, although a systematic difference remains. Within the error, the data corresponds much closer to the curve through the data by Hofman *et al.* than it does to the Hasimoto result.

From our corrected data, we estimated the range over which the raspberry is able to accurately reproduce hydrodynamics interactions ($f < 2.5\%$) in our system. For this particular model we found the criterion to be $L \gtrsim 2.8R_h^T$, which can be extrapolated to other spatial arrangements of the colloids. It is likely that this criterion can be extended to smaller boxes, as we will see in the following and in Ref. [7]. The normalized results for a hollow raspberry lie on top of the filled ones shown in Fig. 6(b) within the error bar. However, the values for the effective hydrodynamic radii R_h^T differ: 3.53σ and 3.47σ for the filled and hollow model, respectively.

We continued our verification of the quality of the filled and hollow raspberry model, by examining hydrodynamic coupling between spheres rotating in unison in the same geometry as before, see Fig. 3(c). Figure 7 shows a comparison of our results to the expression given by Hofman *et al.* [4] for the box-size dependence of the rotational mobility μ_L^R. The procedure used to generate this data is analogous to that outlined for the translational experiments. Using

$$\mu_0^R \equiv \frac{1}{8\pi\eta \left(R_h^T\right)^3} \tag{25}$$

we determined the effective hydrodynamic radius R_h^R from our data. Note that while there is still a systematic component to f, see Fig. 7(b), the agreement between our result and literature is excellent for both models.

This further demonstrates the plausibility of our assertion that the high level of deviation for the translational mobility is caused by the back-force/velocity that is applied homogeneously to the fluid, since a similar correction is not required for the rotational experiments. However, there is a fundamental difference between the experiments. The rotational motion exposes the fluid to constantly varying coupling points (the MD beads), whereas for translational motion the fluid could more easily find a pathway of least resistance.

Again, we observed that the effective hydrodynamic radii obtained for the hollow and filled raspberry differ

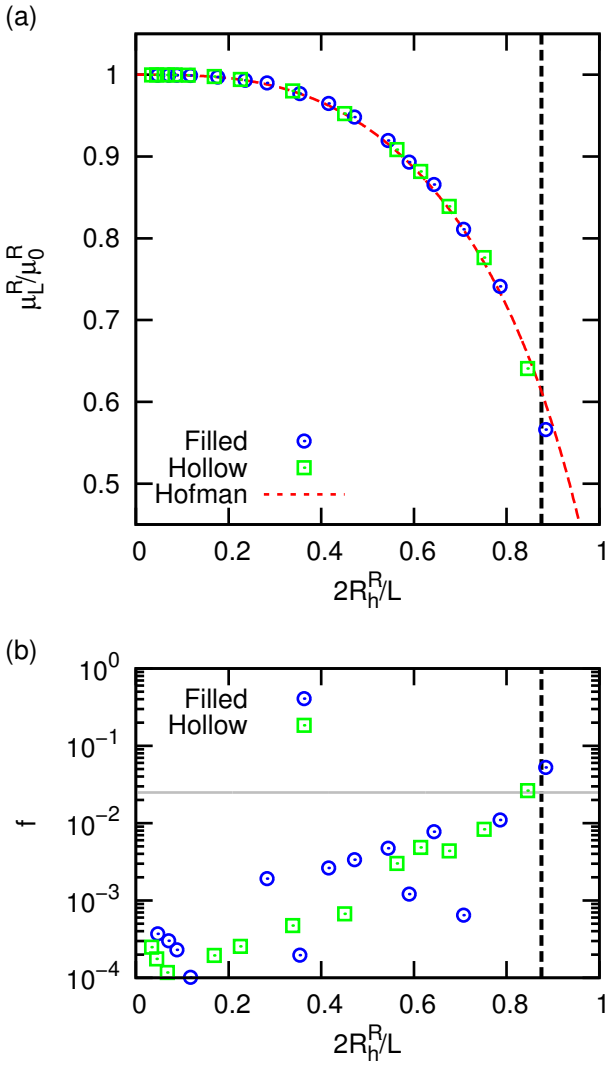

FIG. 7. (color online) (a) The dependence of the particle's rotational mobility μ_L^R (expressed in terms of the bulk rotational mobility μ_0^R) on the inverse box length times the hydrodynamic diameter (twice the hydrodynamic radius R_h^R). The blue circles show results obtained for the filled raspberry and the green squares for the hollow raspberry. The red dashed curve shows the expression given by Hofman *et al.* [4] The vertical dashed black line indicates the value of L, for which the spheres are separated by one lattice spacing. (b) Fractional deviation f as a function of $2R_h^R/L$. The blue circles and green squares indicate the difference between the filled and hollow raspberry and analytic expression, respectively. The gray horizontal line indicates a fractional deviation of 2.5%.

significantly, 3.38σ and 3.54σ, respectively. It should be stressed that the fact that behavior of μ_L^R is the same for both models, does not imply hydrodynamic consistency of the model, when we compare the value of R_h^T and R_h^R for the same model, which we will do next.

To further assess the significance of the difference in effective hydrodynamic radius, we repeated our experi-

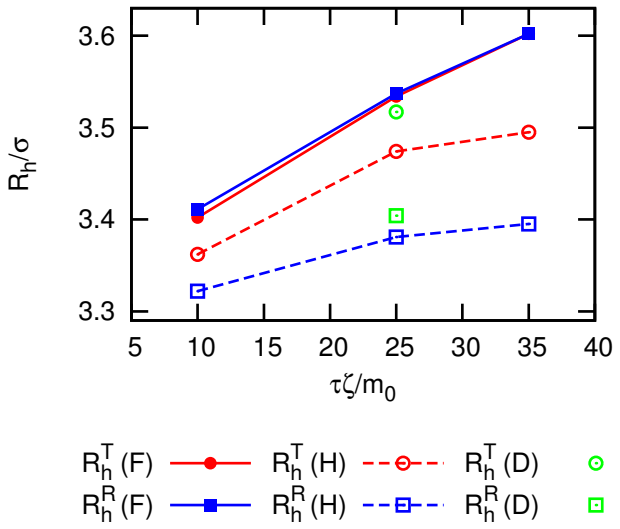

FIG. 8. (color online) The bulk effective hydrodynamic radii (translational R_h^T, rotational R_h^R) for the filled (F), hollow (H), and dense (D) raspberry models, respectively, as a function of the friction coefficient expressed in LB units (time τ and mass m_0).

ments for two other values of the bare friction ζ_0. The results for the box-size dependence were in quantitative agreement. Our results for the hydrodynamic radii are summarized in Fig. 8. These effective hydrodynamic radii were obtained, as before, by extrapolation to the bulk value of the mobility and utilizing the Stokes-Einstein relation. Note that the translational and rotational radius of the hollow raspberry differ substantially. This result is in agreement with the findings of Ollila *et al.* [26, 27] The mismatch occurs for all values of the friction coefficient that we examined.

We also performed experiments with a hollow raspberry that had the same number of surface beads as the total number of beads used in the filled raspberry – we refer to this model as the 'dense' raspberry. This allowed us to examine the hypothesis that we simply obtained an increased effective friction with greater bead numbers used in the filled raspberry, leading to a better match between rotational and translational hydrodynamic radius. [27] A similar discrepancy between R_h^T and R_h^R was found for the dense model, see Fig. 8. In fact, the deviation is slightly increased. This can be attributed to an overall improvement of the coupling, which forces the translational radius towards the no-slip value more quickly than that of the rotation. In the limit of much greater numbers of coupling points, the dense shell and filled sphere's porosity should vanish and give correspondence to the solid-sphere result. [26]

Finally, we examined the fluid-particle coupling to determine the cause of the inconsistency between the effective hydrodynamic radii that were obtained using the

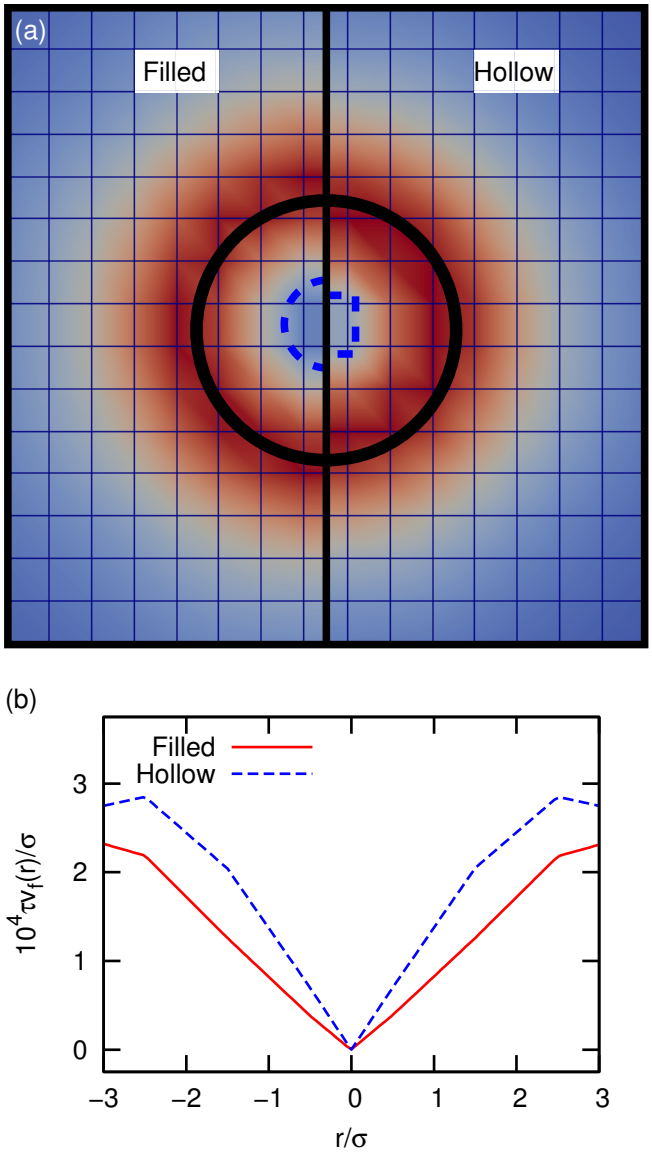

FIG. 9. (color online) Comparison of the flow field around a filled and hollow raspberry, respectively, undergoing a constant rotation. (a) Two dimensional plane through the center of the sphere with a normal that is parallel to the axis of rotation. The result for the filled raspberry is shown on the left and for the hollow variant on the right. The color coding gives the magnitude of the fluid velocity on the grid (blue lines). The thick black circle roughly indicates the position of the coupling points (at $|\mathbf{r}| = R$). The dashed blue semi circle and half square serve as guides to the eye for the structure of the flow field inside the raspberry. (b) Magnitude of the fluid velocity $v_f(r)$ – expressed in MD units of time, τ, and position σ – as a function of position r along the black vertical divide in (a). Only the value inside of the raspberry is shown for the filled (red, solid) and hollow (blue, dashed) particle.

hollow raspberry model. Figure 9(a) shows the flow field around a hollow and filled spherical raspberry, rotating at constant angular velocity about the axis pointing into the

page. From the flow field it becomes apparent that the coupling of the raspberry to the fluid has more lattice artifacts for the hollow raspberry than for the filled one (is less smooth), indicating poorer coupling. We quantified this difference further by examining the fluid velocity inside the particle, see Fig. 9(b). While the filled raspberry shows a linear increase in the velocity with the distance from the center (similar to the so-called 'Rankine vortex state'), the hollow raspberry shows a clear kink in the velocity profile. This kink can be attributed to the diminished fluid-particle coupling away from the shell of MD beads. Effectively, the hollow shell raspberry achieves a low Brinkman length only close to the shell, whereas the filled raspberry achieves low permeability throughout.

B. Dumbbell in a Simple Cubic Crystal

Thus far, we have concentrated on the quality of the raspberry approximation for convex objects, namely the specific case of a spherical particle. In order to assess the raspberry model's ability to capture the hydrodynamic properties of a non-convex particle, we considered two dumbbell-shaped raspberries, as shown in Fig. 2. We took care to create a raspberry model for which the two spheres touch, when the effective hydrodynamic radius of the MD beads is taken into account, see Fig. 2 (left). Note that for a dumbbell-shaped particle the hydrodynamic mobility tensor (HMT) has a diagonal form, with translational mobilities in the top-left 3×3 block (submatrix) and rotational ones in the lower-right 3×3 block. There are no cross-coupling terms due to symmetry considerations. [51, 52]

Our results for the dumbbell particles are qualitatively similar to the ones shown for the spherical colloid discussed above. Namely, we found the box-size dependence to be of the form $\mu^X_{L,i} = \mu^X_{0,i}\left(1 + a_i/L + b_i/L^3\right)$, with X either R or T and i either $\perp$ or $\parallel$, and a_i and b_i coefficients. However, we could not compare our results to analytic calculations, since, to the best of our knowledge, such expressions have not been formulated for dumbbell-shaped particles. We therefore considered the extrapolated bulk mobility coefficients only. Using both quiescent and thermalized simulations we verified that the HMT had the expected form. In particular, all off-diagonal coefficients were orders of magnitude smaller than the diagonal elements and zero within the error bars. Moreover, we found that for both the translational and rotational mobility sub-matrices, the two entries corresponding to perpendicular motion were equal (within the error) and the parallel component was larger, as expected. Table I lists these mobility coefficients. In order to de-dimensionalize the results, we divided the mobility coefficients by the translational and rotational mobility coefficient of a sphere with radius $R = 3\sigma$, respectively.

To validate our model for the simulation of anisotropic non-convex particles, we compared our data with the results obtained using the *HYDROSUB* and *HYDRO++* program. [53, 54] These are tools used to evaluate the hydrodynamic properties of macromolecules and have been successfully utilized in comparisons to experimental data for solid anisotropic colloids. [55] We determined the HMT using the methods of Refs. [53, 54] for dumbbells consisting of two spheres with radii $R = 1.0$ μm at positions $(\pm 1.0, 0, 0)$ μm (touching) and $(\pm 0.714, 0, 0)$ μm (separated), respectively, in a fluid of viscosity 10^{-3} $\mathrm{kg\,m^{-1}\,s^{-1}}$ and density 10^3 $\mathrm{kg\,m^{-3}}$ with temperature $T = 293.15$ K. We assumed that the particle has the same density as the fluid. The numerical algorithm is parametrized as follows: $H = 26$, $H_{\max} = 1.5 \cdot 10^7$, $R_{\max} = 80.0 \cdot 10^{-8}$, and $N_{\mathrm{TRIALS}} = 10{,}000$; which are internal commands. The number of intervals for the distance distribution was set to 30. By applying the same numerical parameters to the case of a single sphere we obtained the reference data used to normalize the result.

Method	$\mu^T_\parallel/\mu^T_0$	$\mu^T_\perp/\mu^T_0$	$\mu^R_\parallel/\mu^R_0$	$\mu^R_\perp/\mu^R_0$
$d = 7\sigma$ / $d = 2.00$ μm				
Rasp. (H)	0.78 ± 0.01	0.70 ± 0.01	0.61 ± 0.01	0.28 ± 0.01
Rasp. (F)	0.77 ± 0.01	0.69 ± 0.01	0.55 ± 0.01	0.27 ± 0.01
[53, 54]	0.77 ± 0.01	0.70 ± 0.01	0.55 ± 0.01	0.27 ± 0.01
$d = 5\sigma$ / $d = 1.43$ μm				
Rasp. (H)	0.83 ± 0.01	0.75 ± 0.01	0.67 ± 0.01	0.39 ± 0.01
Rasp. (F)	0.82 ± 0.01	0.74 ± 0.01	0.59 ± 0.01	0.36 ± 0.01
[53, 54]	0.82 ± 0.01	0.75 ± 0.01	0.60 ± 0.01	0.37 ± 0.01

TABLE I. Comparison for a dumbbell-shaped particle between the results obtained using the raspberry model – both hollow (H) and filled (F) – and *HYDROSUB*/*HYDRO++* [53, 54] for the translational (T) and rotational (R) mobilities in the direction parallel ($\parallel$) and perpendicular ($\perp$) to the main axis in bulk fluid. The mobilities are normalized by the bulk values for a sphere with the same radius as one of the spheres comprising the dumbbell.

The results of this comparison are summarized in Table I, in which we give the mobilities for the filled and hollow raspberry, as well as the ones determined using the methods of Refs. [53, 54]. The agreement for the bulk mobilities is excellent for the translational bulk mobilities of all three data sets. However, it is clear that for the hollow raspberry there is a significant difference in the rotational mobility ratio with respect to the result for the filled and *HYDROSUB*/*HYDRO++* simulations that lies well outside of the error bar of the average of the latter two. This confirms that our 'filling + fitting' procedure is effective for more complex (non-convex) geometries, as expected.

IV. DISCUSSION

In Section III we have demonstrated that our 'filling + fitting' formalism leads to excellent agreement between established theoretical and numerical results for the hydrodynamic behavior of convex and non-convex solid par-

ticles. By 'filling and fitting' one significantly improves the agreement between the effective hydrodynamic radii obtained by translational and rotational experiments, respectively, allowing the point-coupling LB model to describe solid particles. The improvement is related to a reduced permeability throughout the particle – in line with the findings of Ref. [26]. The hollow-shell raspberry achieves this only locally. [14, 15, 27, 29] In this section we discuss this discrepancy between the effective hydrodynamic radii in more detail and place our work in the context of previous studies.

The fractional difference in hydrodynamic radii of approximately $0.1\sigma/3.4\sigma = 0.03$ for the hollow raspberry may seem perfectly acceptable for most applications. However, one should be careful, since this small fraction can lead to a 10% discrepancy between the expected translational and rotational mobility; had we assumed the effective hydrodynamic radius for rotational motion to be the same as that for translational motion. In processes involving both translation and rotation, this could lead to significant deviation from the desired behavior.

A closer examination of the data presented in the original raspberry paper by Lobaskin and Dünweg [14] shows that the trends in matching to the results of Refs. [4, 8–11] with effective hydrodynamic radii observed in our work, are captured by their data points. Lobaskin and Dünweg erroneously assumed that the radius of the particle was the same as the radius R at which they positioned their MD beads. However, within the numerical uncertainty present in their results and the computational abilities of the time, this extrapolation to bulk was completely justifiable. By re-examining the data points of Ref. [14], we conclude that it is possible to fit the following bulk mobilities

$$\mu_0^T = (0.97 \pm 0.02)\frac{k_\mathrm{B}T}{6\pi\eta R}; \tag{26}$$

$$\mu_0^R = (0.90 \pm 0.02)\frac{k_\mathrm{B}T}{8\pi\eta R^3}. \tag{27}$$

This indicates that there is indeed an effective radius, $R_h^T = (1.03 \pm 0.02)R$ and $R_h^R = (1.03 \pm 0.01)R$, but the data is not of sufficient quality to assess whether there is a difference between the effective translational and rotational hydrodynamic radius in their measurements.

Chatterji and Horbach [15] carried out a more thorough examination of the effective translational hydrodynamic radius. However, they did not provide results for the rotational hydrodynamic radius, they only comment on having carried out such experiments. Our results in Fig. 8 for the value of R_h^T for the hollow raspberry are in quantitative agreement with Ref. [15]. We therefore deem it likely that a similar discrepancy would be present in the data of Ref. [15], especially considering our observations and those of Refs. [26, 27].

Finally, Poblete *et al.* [22] did not report a difference in the bulk hydrodynamic radii using their MPCD method for a hollow raspberry. They instead found agreement between the two. However, it is unclear how accurately Poblete *et al.* could extrapolate their results to the bulk value, as in MPCD one always works with thermalized and therefore noisy data. In addition, it is not obvious how large the effect ($R_h^T \neq R_h^R$) would be for their high-speed-of-sound systems. Furthermore, the grid-shifts that are typically applied in MPCD to restore Galilean invariance, may substantially reduce any such lattice-discretization and porosity effects.

The inconsistency between the translational and rotational mobility in the raspberry model was first pointed out by Ollila *et al.* [26, 27] In Ref. [26] it was contended that these inconsistencies are representative of the properties of the point-coupling method. Namely, that the objects modeled using this formalism are porous. Ollila *et al.* argue that this porosity leads to problems when using this type of model to describe solid objects. Especially models that fit for this value should be considered suspect according to Ref. [26], as there may be inconsistencies in the fitted hydrodynamic radius for various hydrodynamic experiments. This assessment may seem in direct contradiction of our observations. However, Ollila *et al.* do not exclude the possibility of finding numerical parameters for which a quality fit can be made. We have shown here, as well as in Ref. [7], that our 'fitting + filling' formalism works well to match the simulations to analytic results for solid particles over a wide range of parameters. That is we obtained numerically consistency for physically relevant hydrodynamic experiments.

It should be noted that the excellent agreement shown between the simulation results and analytic expressions for porous spheres in Ref. [26] is not without caveats. In particular, Ollila *et al.* indicate that it is necessary to use particle radius for the coupling points that is 'incommensurate' with the lattice to obtain the excellent correspondence for the translational properties of the porous particles without fitting. Due to the properties of the interpolation scheme, this incommensurability criterion and the subsequent choice of a particle radius that yields correspondence, can be treated on the same footing as a fit parameter. Moreover, Ollila *et al.* require an effective hydrodynamic radius to obtain an equally excellent correspondence for the rotational properties of their particles.

We have performed our simulations with both stationary and moving particles at positions and in directions both commensurate and incommensurate with the lattice. In all these experiments, we did not find a sizable change in the effective radii, nor a breakdown of the correspondence between the two. We thus argue that our 'filling + fitting' method is a cleaner and more forthright way of approaching matching the simulations to analytic results for solid objects. In addition, we believe that an equally excellent correspondence between theory and simulations could have been achieved in Ref. [26], by dropping the incommensurability criterion and fitting for both effective hydrodynamic radii.

Finally, in relation to the work of Refs. [26, 27] another observation should be made. In both papers the number

of coupling points used to obtain correspondence between the theory and simulations is rather large. Such a high number of points is acceptable in addressing questions of a fundamental nature, but it may prove problematic in performing simulations with high numbers of particles, as is typical for self-assembly and crystallization studies. [56]

The algorithm may become prohibitively expensive for such a high number of coupling points. Lowering the overall number of coupling points and specifically their local density is of particular relevance to GPU-based LB implementations. The force applied to the nodes of the LB grid by a coupling point is calculated using so-called 'atomicAdd' operations. These operations can be used to avoid race conditions that arise from colliding memory requests. However, for high numbers of particles close to a specific LB node (high coupling-point density), the use of the atomicAdd operation can cause the program to slow down significantly. Therefore, reducing the number of local coupling points is of paramount importance and our 'filling + fitting' procedure is thus numerically favorable to models that require a higher coupling-point density.

With regards to the filling procedure, we obtained reasonable consistency for the translational and rotational mobility for the number of MD beads that we added to the interior of the particle. However, it is quite likely that similar results may be achieved by adding far fewer particles to the interior of the model, which will further improve the computational performance of a simulation. It is worth noting that by increasing the radius of the raspberry, the problem may be substantially reduced as well, as the difference between the effective radii becomes less important for larger R. The need for filling, increasing R, or both should be examined on a per-simulation-study basis.

Finally, a comment on the short-time behavior of the raspberry particles is appropriate. As originally shown in Ref. [14], the Ahlrichs and Dünweg interpolated point-coupling scheme [13] has problems in reproducing the short-time properties of the (A)VACF that are expected for a solid no-slip particle [34] or even a porous colloid, [44] due to the presence of an unphysical coupling regime. The correct zero-time value of $C_L^T(0) = 3k_\mathrm{B}T/m$ is achieved, but there is no decay to $C_L^T(t > 0) = 3k_\mathrm{B}T/m^*$, with m^* the virtual mass, over a time scale related to the propagation of sound. [34] Instead, a much lower plateau value for $C_L^T(t > 0)$ is reached. Felderhof [44] has pointed out that the secondary (virtual mass) regime is not present in a porous colloid, which is thus in agreement with our findings and contradicts the earlier report by Lobaskin and Dünweg. [14] However, the behavior predicted in Ref. [44] is also not accurately captured, since the unphysical coupling regime interferes with the onset of the proper short-time decay.

It has been suggested that the modified coupling scheme by Mackay *et al.* [28] may resolve these issues. However, examination of the VACFs reported in Ref. [29] reveal that the double exponential-type decay shown in their fluid-mass dominated result is not captured by the result of Ref. [34], as is reported in Ref. [29] (but not demonstrated using fitting procedures). This is, again, expected on the basis of the results by Felderhof [44]. Unfortunately, it is also not clear that the predictions of Ref. [44] are more accurately reproduced. Furthermore, an analysis of the results of the oscillatory experiments in Ref. [26] does not yield significant additional insight into the short-time quality of the Mackay *et al.* algorithm. In particular, it is unclear whether this algorithm was used in this work. Also, the period of the oscillation is sufficiently long to obfuscate any short-time discrepancies that may be present.

V. CONCLUSION AND OUTLOOK

Summarizing, we have re-examined the properties of the hybrid LB and Langevin MD scheme for simulating colloids developed by Lobaskin and Dünweg, [14] the so-called 'raspberry' model. We studied this model using a variety of classic fluid dynamics experiments that predominantly focused on the long-time mobility properties of these particles. We considered the hydrodynamic properties of spherical raspberries, as well as dumbbell-shaped raspberry particles in the low Reynolds number limit. Our results show that the proper solid-particle mobility in this limit is reproduced to a surprising degree of accuracy over a wide range of viscosities for both convex and non-convex particle shapes.

From our combined data we can draw the following conclusions concerning the quality of the raspberry model and our 'filling + fitting' procedure to match its hydrodynamic properties to that of a solid object in a low-Reynolds-number fluid.

- Using a raspberry model to approximate a particle's coupling to an LB fluid gives rise to an effective hydrodynamic radius. This effective radius must be properly taken into account in matching to the (experimental) system of interest. Our result is in agreement with the findings of Chatterji and Horbach. [15] We have commented on the claims of Ollila *et al.* [26, 27] that correspondence between simulations and theory can be obtained without such a fit parameter and we have argued that their result could be a result of a fortuitous choice of particle radius.

- The short-time properties of a no-slip or permeable colloid are not faithfully reproduced by the Ahlrichs and Dünweg interpolated point-coupling scheme, [13] as was first pointed out in Ref. [14].

- The traditional 'hollow' raspberry model – an empty shell of MD coupling beads that describes the particle's surface – gives rise to a discrepancy between the translational and rotational effective

hydrodynamic radius. This effect was first pointed out by Ollila *et al.* [26, 27] and discussed in the context of porous particle dynamics.

- We find that the aforementioned mismatch, when considered in the context of reproducing the hydrodynamic behavior of a solid particle, can be reduced within an acceptable numerical tolerance by 'filling' the raspberry and 'fitting' for the effective hydrodynamic radius. This is not in disagreement with the assessment of Ollila *et al.* [26] that such a filling procedure is inherently problematic. Our result merely demonstrates that for reasonable LB parameters the hydrodynamic properties of a solid particle can be effectively matched and to within a far higher tolerance than is possible for the hollow variant.

- The 'filling + fitting' procedure can be used to improve the raspberry model's ability to simulate both convex and non-convex solid particles. We verified this for the specific case of a dumbbell-shaped particle, but our results may be safely extrapolated to more complicated shapes. However, the effective hydrodynamic radius of the raspberry must be properly taken into account. That is, the MD beads must be positioned in such a way that the effective hydrodynamic hull, which forms around these points, approximates the shape of the particle of interest.

- The result of Ollila *et al.* [27] suggest that a regime can be found for which the hull is sufficiently shrunk that it matches with the imposed position of the coupling points. However, a prohibitive number of coupling points may be required to achieve this condition. This is especially problematic for GPU-based algorithms. Our 'filling + fitting' procedure allows us to use a substantially reduced number of coupling points and still obtains excellent numerical agreement.

- The force and velocity experiments traditionally performed to determine the translational mobility in a cubic geometry with periodic boundary conditions are problematic for small boxes compared to the particle size. The back force/velocity density that must be applied to the fluid to maintain zero center of mass velocity, leads to difficulties in interpretation the mobility data that is obtained from these experiments. We find that the net/effective force acting on the particle is given by the applied force minus the back force density integrated over the volume that the raspberry occupies. Utilizing this net force gives a better match with numerical results for the solution to Stokes' equations for solid particles in this geometry. [4, 8, 9] A similar consideration applies to the velocity experiment, where it leads to the observed systematic (albeit small) disagreement between the thermal and quiescent data at intermediate and long time scales. A possible solution to this problem is to identify the node locations at which the particle is found and to only apply the properly-rescaled counter force elsewhere.

From the above, it becomes clear that the raspberry model is an excellent way to approximate long-time regime of the fluid-particle coupling for a solid object in an LB algorithm. However, there remain several open problems to be addressed in future studies. We have shown that the short-time behavior of the raspberry model (for the LB parameters used in this manuscript) is quite different from the low Reynolds number solution to Stokes' equations. [34, 44] This raises the question of how accurately the short-time regime of colloid dynamics can be captured using the raspberry or any point-coupling model. An faithful reproduction of such short-time processes would be relevant for, e.g., nucleation and crystallization. Despite this concern, our analysis stresses the power of the original our 'filled + fitted' raspberry model as a means to approximate translational as well as rotational fluid-particle coupling.

ACKNOWLEDGEMENTS

J.d.G. acknowledges financial support by a "Nederlandse Organisatie voor Wetenschappelijk Onderzoek" (NWO) Rubicon Grant (#680501210). We thank the "Deutsche Forschungsgemeinschaft" (DFG) for financial funding through the SPP 1726 "Microswimmers – from single particle motion to collective behavior". We are also grateful to O. Hickey and S. Kesselheim for useful discussions.

[1] L. Euler, Mem. Acad. Sci. Inst. Berlin **11**, 274 (1757).
[2] C. Navier, Mem. Acad. Sci. Inst. France **6**, 389 (1822).
[3] G. Stokes, Trans. Cambridge Phil. Soc. **8**, 287 (1849).
[4] J. Hofman, H. Clercx, and P. Schram, Physica **268**, 353 (1999).
[5] J. Giddings, Separ. Sci. Technol. **13**, 241 (1978).
[6] R. Noel, K. Gooding, F. Regnier, C. Orr, and M. Mullins, J. Chromatogr. A **166**, 373 (1978).
[7] J. de Graaf, T. Peter, L. Fischer, and C. Holm, J. Chem. Phys. **submitted**, (2015).
[8] H. Hasimoto, J. Fluid Mech. **5**, 317328 (1959).
[9] A. Zick and G. Homsy, J. Fluid Mech. **115**, 13 (1982).
[10] H. Brenner, J. Colloid and Interface Sci. **32**, 141 (1970).
[11] M. Zuzovsky, P. Adler, and H. Brenner, Phys. Fluids **26**, 1714 (1983).

[12] B. Dünweg and A. Ladd, Lattice boltzmann simulations of soft matter systems, in Advanced Computer Simulation Approaches for Soft Matter Sciences III, edited by C. Holm and K. Kremer, volume 221 of Adv. Polymer Sci., pages 89–166, Springer (Berlin/Heidelberg), 2009.

[13] P. Ahlrichs and B. Dünweg, J. Chem. Phys. **111**, 8225 (1999).

[14] V. Lobaskin and B. Dünweg, New J. Phys. **6**, 54 (2004).

[15] A. Chatterji and J. Horbach, J. Chem. Phys. **122**, 184903 (2005).

[16] A. Ladd, J. Fluid Mech. **271**, 285 (1994).

[17] C. Aidun and Y. Lu, J. Stat. Phys. **81**, 49 (1995).

[18] V. Lobaskin, B. Dünweg, M. Medebach, T. Palberg, and C. Holm, Phys. Rev. Lett. **98**, 176105 (2007).

[19] V. Lobaskin, D. Lobaskin, and I. Kulić, Eur. Phys. J. Spec. Top. **157**, 149 (2008).

[20] S. Raafatnia, O. Hickey, and C. Holm, Phys. Rev. Lett. **113**, 238301 (2014).

[21] M. Belushkin, R. Winkler, and G. Foffi, J. Phys. Chem. B **115**, 14263 (2011).

[22] S. Poblete, A. Wysocki, G. Gompper, and R. Winkler, Phys. Rev. E **90**, 033314 (2014).

[23] J. Sané, J. Padding, and A. Louis, Phys. Rev. E **79**, 051402 (2009).

[24] F. Lugli, E. Brini, and F. Zerbetto, J. Phys. Chem. C **116**, 592 (2012).

[25] J. Zhou and F. Schmid, Eur. Phys. J. E **36** (2013).

[26] S. Ollila, T. Ala-Nissila, and C. Denniston, J. Fluid Mech. **709**, 123 (2012).

[27] S. Ollila, C. Smith, T. Ala-Nissila, and C. Denniston, Multiscale Model. Simul. **11**, 213 (2013).

[28] F. Mackay, S. Ollila, and C. Denniston, Comput. Phys. Commun. **184**, 2021 (2013).

[29] F. Mackay and C. Denniston, J. Comput. Phys. **237**, 289 (2013).

[30] J. Deutch and B. Felderhof, J. Chem. Phys. **62**, 2398 (1975).

[31] B. Felderhof, Physica A **80**, 63 (1975).

[32] H. J. Limbach, A. Arnold, B. A. Mann, and C. Holm, Comp. Phys. Comm. **174**, 704 (2006).

[33] A. Arnold et al., ESPResSo 3.1 — Molecular Dynamics Software for Coarse-Grained Models, in Meshfree Methods for Partial Differential Equations VI, edited by M. Griebel and M. A. Schweitzer, volume 89 of Lecture Notes in Computational Science and Engineering, page 1, Springer, 2013.

[34] R. Zwanzig and M. Bixon, J. Fluid Mech. **69**, 21 (1975).

[35] D. Roehm and A. Arnold, Eur. Phys. J. ST **210**, 73 (2012).

[36] D. d'Humières, I. Ginzburg, M. Krafczyk, P. Lallemand, and L.-S. Luo, Philos. Trans. A Math. Phys. Eng. Sci. **360**, 437 (2002).

[37] R. Adhikari, K. Stratford, M. E. Cates, and A. J. Wagner, Euro. Phys. Lett. **71**, 473 (2005).

[38] B. Dünweg, U. Schiller, and A. Ladd, Phys. Rev. E **76**, 036704 (2007).

[39] B. Dünweg, U. Schiller, and A. Ladd, Comp. Phys. Commun. **180**, 605 (2009).

[40] J. Padding and A. Louis, Phys. Rev. E **74**, 031402 (2006).

[41] A. Louis, Faraday Discuss. **144**, 323 (2010).

[42] J. Ramirez, S. Sukumaran, B. Vorselaars, and A. Likhtman., J. Chem. Phys. **133**, 154103 (2010).

[43] E. Hauge and A. Martin-Löf, J. Stat. Phys. **7**, 259 (1973).

[44] B. Felderhof, J. Chem. Phys. **140**, 134901 (2014).

[45] J.-P. Hansen and I. McDonald, Theory of Simple Liquids, Academic Press (London), 2nd edition, 1986.

[46] E. Hinch, J. Fluid. Mech. **72**, 499 (1975).

[47] B. Cichocki and R. Jones, Physica A **258**, 273 (1998).

[48] M. Friese, T. Nieminen, N. Heckenberg, and H. Rubinsztein-Dunlop, Nature **394**, 348 (1998).

[49] B. Grzybowski, H. Stone, and G. Whitesides, Nature **405**, 1033 (2000).

[50] B. Grzybowski, X. Jiang, H. Stone, and G. Whitesides, Phys. Rev. E **64**, 011603 (2001).

[51] H. Brenner, J. Colloid Sci. **20**, 104 (1965).

[52] H. Brenner, J. Colloid Interface Sci. **23**, 407 (1967).

[53] J. G. de la Torre and V. Bloomfield, Q. Rev. Biophy. **14**, 81 (1981).

[54] J. G. de la Torre, G. del Rio, and A. Ortega, J. Phys. Chem. B **111**, 955 (2007).

[55] D. Kraft et al., Phys. Rev. E **88**, 050301 (2013).

[56] D. Roehm, S. Kesselheim, and A. Arnold, Soft Matter **10**, 5503 (2014).